Available online at www.sciencedirect.com
ScienceDirect
Ultramicroscopy 107 (2007) 374–381
ultramicroscopy
www.elsevier.com/locate/ultramic

Charge defects glowing in the dark

Bin Deng*, Laurence D. Marks, James M. Rondinelli

Department of Materials Science and Engineering, Northwestern University, Evanston, IL 60208-3108, USA

Received 5 June 2006; received in revised form 15 September 2006; accepted 10 October 2006

Abstract

We investigate the effects of local charge defects in HREM imaging, using electron densities calculated by density functional methods. As a model of a planar interface with a local charge defect we use the polar MgO (1 1 1)$-\sqrt{3}\times\sqrt{3}R30^\circ$ surface, which has an additional hole per surface unit cell. A complimentary example, the non-polar MgO (1 0 0) surface that has no local charge defect is simulated for comparison. We show that the contrast due to local charge defects is rather high, and suggest that they should be directly observable.

PACS: 68.37.−d; 68.37.Lp; 07.05.Pj; 73.20.−r

Keywords: Charge density; Structure factors; Charge transfer; Charge defects; HREM

1. Introduction

There are currently numerous methods for obtaining local structural information using transmission electron microscopy. For example, high-resolution electron microscopy (HREM) and Z-contrast STEM are routinely used to study atomic arrangements at interfaces in materials. Most studies with HREM and Z-contrast have been focused on achieving atomic resolution (1–2 Å) and accurately locating atomic positions. While atomic positions are important, there is much more one would like to know. For instance, if one knew the electron density, in many respects one would not need any further information since, at least in principle, the density fully determines most of the properties including the positions of the nuclei. Electron energy loss spectroscopy has demonstrated that it can be performed with atomic-scale resolution, but this is not a direct measure of the electron density in a material, rather a measure of the local joint-density of states. Electron-diffraction techniques have been recently shown to be successful in determining electron charge density. With convergent beam electron diffraction, bonding charge and charge transfer can be evaluated in bulk materials with the accurate measurement (0.1%) of structure factors [1–13]. Despite experimentally measured surface diffraction intensities having relatively poor accuracy (1–10%), it is also possible to obtain charge transfer information between surface atoms [14,15]. What all of these approaches have in common is the use of electron diffraction to observe charge redistribution in reciprocal space, which only permits the observation of an average result not any local changes. A question then naturally arises: can we "see" charge transfer and local charge defects (i.e. localized charge compensating hole or electron states) directly by imaging in real space, particularly at the atomic level? Charge transfer is very common at interfaces, around vacancy clusters, etc. and direct imaging of these would open up new frontiers for electron microscopy.

In our previous studies, we have shown that charge transfer in a bulk material can lead to a difference of 5–7% in the electron structure factors and that these effects should be detectable in HREM images [16]. In the present work, we will investigate the feasibility of directly imaging local charge defects by HREM. As models of simple planar defects, we will use as two representative cases, a polar surface and a non-polar surface, both simulated in profile mode. The first model is the reconstructed MgO (1 1 1)$-\sqrt{3}\times\sqrt{3}R30^\circ$ surface, denoted as MgO Rt3 for simplicity. The MgO Rt3 surface structure is magnesium

*Corresponding author. Tel.: +1 847 491 7809; fax: +1 847 491 7820.
E-mail address: b-deng@northwestern.edu (B. Deng).

0304-3991/$ - see front matter © 2006 Elsevier B.V. All rights reserved.
doi:10.1016/j.ultramic.2006.10.001

(Mg) terminated with two Mg vacancies located in the first layer relative to the simple bulk terminated surface [14,15]. Our previous studies indicate that an additional electron hole per surface unit cell is required for charge compensation and that this is primarily localized in the second O layer. The second model used is the non-polar MgO (1 0 0) surface, for which there are only very minimal changes in the electron density at the surface.

The simulations, which we describe, are similar to the imaging configuration that is routinely used for grain boundaries and other defects where local charge defects may be present. We find strong theoretical evidence that one should, in practice, be able to directly observe effects from charge transfer and charge defects in a material by HREM imaging.

2. Numerical method

Multislice image simulations were performed on projected potentials derived from three sets of X-ray structure factors. The first two sets are calculated from neutral atoms, denoted as F^x_{neu}, and bulk ions, F^x_{ion}, from fitted atomic scattering factors using a recent analytical form as a linear combination of five Gaussians:

$$f^x(s) = \sum_{i=1}^{5} a_i \exp(-b_i s^2) + c, \tag{1}$$

where a_i, b_i, and c are tabulated parameters, and s is $\sin(\theta)/\lambda$. The fitting parameters for the neutral atoms (Mg and O) charge density [17] and the self-consistent bulk (MgO) ion charge density [18] are available in the literature.

The third set of structure factors (F^x_{scf}) was calculated by full-potential density functional theory (DFT) implemented in the WIEN2K program [19,20]. The MgO Rt3 surface structure was modeled by a slab of 13 layers (35 atoms), separated by a vacuum slab of 14 Å in length. The unit cell contains 17 Mg atoms and 18 O atoms at fully relaxed positions using a GGA potential [21]. In a similar fashion, the MgO (1 0 0) non-polar surface was modeled by a slab of 12 layers, separated by a vacuum of 21 Å in length, which was also fully relaxed using WIEN2K. In both cases, the DFT equilibrium lattice parameters for MgO were used which are about 1% larger; this is a typical value and should have almost no effect on any of the conclusions.

The X-ray structure factors in all three cases were directly converted to electron structure factors using the Mott–Bethe formula. To be consistent, $F^{\mathrm{e}}_{\mathrm{neu}}$, $F^{\mathrm{e}}_{\mathrm{ion}}$, and $F^{\mathrm{e}}_{\mathrm{scf}}$ refer to the electron structure factors generated from F^x_{neu}, F^x_{ion}, and F^x_{scf}, respectively. The electron structure factors were then projected along the directions of interest (here [1 1 0]) into slices of thickness less than 2.0 Å along the beam direction by

$$V_{\mathrm{p}}(x,y) = \frac{1}{\Omega}\sum_{h,k} F^{\mathrm{e}}(h,k,0)\exp(-2\pi \mathrm{i}(hx+ky)), \tag{2}$$

where $F^{\mathrm{e}}(h,k,0)$ is the projected structure factor. Then the unit cell is cut into thinner sub-slices with a thickness less than 2 Å. Each slice has the same projected potential $V_{\mathrm{p}}(x, y)/n$, where n is the number of slices for one unit cell. Although we recognize that this method ignores conventional high-angle higher-order Laue zone effects, they should in principle be negligible under normal imaging conditions. A slightly more severe approximation is neglect of the higher-order Laue Zone contribution to the 1×1 reflections (nominally 1/3(422) spots) for the MgO Rt3 (e.g. Ref. [22]), although these are relatively weak intensities. A constant temperature factor of 0.25 Å^2 for all atoms was used in the simulations, and applied as a simple multiplier in reciprocal space.

For a rigorous investigation of the experimental feasibility of detecting charge defects, two different sets of microscope parameters were used in order to evaluate defocus effects on the image contrast of the charge defects. One is for a conventional H9000 microscope with $C_{\mathrm{s}} = 0.9$ mm, accelerating voltage = 300 kV, beam convergence = 0.68 mrad, and defocus spread = 80 Å, and the other for an aberration-corrected Jeol 2200FS microscope [23] with $C_{\mathrm{s}} = 0.05$ mm, accelerating voltage = 200 kV, beam convergence = 0.1 mrad, and defocus spread = 20 Å.

3. Results

It is well known that a linear Fourier transform relates the structure factors to the charge densities in a material; as a result, different structure factors should represent different charge densities and electrostatic potentials. In most routine HREM image simulations, neutral atom structure factors are used, which ignores the charge redistribution in the material. Another set of structure factors that are routinely used come from self-consistent field (scf) calculations decomposed from the charge density of the crystal. Throughout this paper, we will reference the simulated images as I(src), according to the original structure factor source data (src) used to generate the images, i.e. neu, ion, or scf. The two structures we used are shown in Figs. 1(a) and 2(a). In our simulations, image difference maps were used to understand and quantify the local changes, as shown in Figs. 1(c), (d), 2(c) and (d). The standard deviation (σ) of an image was used as a quantitative measure of the contrast. For the MgO Rt3 structure, the primary changes observed in the atomic positions and charge density occur in the top two or three surface layers, since those near the center of the slab describe the bulk material very well. In our simulation, we have designated the three top layers of the slab as surface layers and the remaining layers as bulk for both MgO Rt3 and MgO (1 0 0) structures. Typical HREM profile images of the MgO Rt3 and the MgO (1 0 0) structures are shown in Figs. 1(b) and 2(b), respectively.

3.1. Image simulation from neutral and ion structure factors

The contrast difference was calculated from the profile images, which are simulated, by neutral atom and ion structure factors at various defocus values (Supplementary

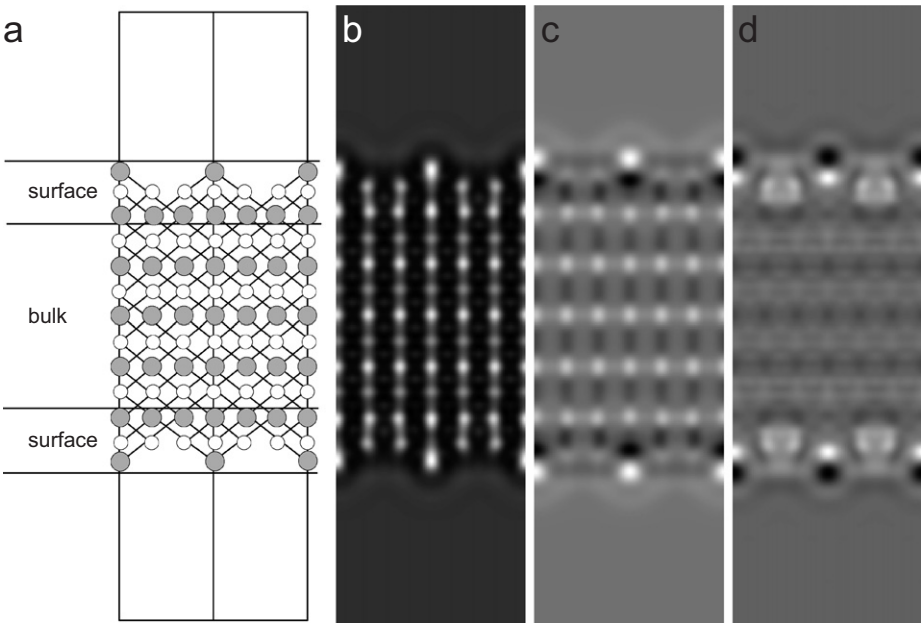

Fig. 1. The 13-layer structure of MgO Rt3 (a) and its image I(scf) (b), image I(scf-neu) (c), and image I(scf-ion), for an aberration corrected Jeol2200FS. The image ranges are 0.8330 to 1.4255 for (b), −0.0400 to 0.0457 for (c), and −0.0502 to 0.0472 for (d). The thickness is 10 unit cells thick (about 52 Å).

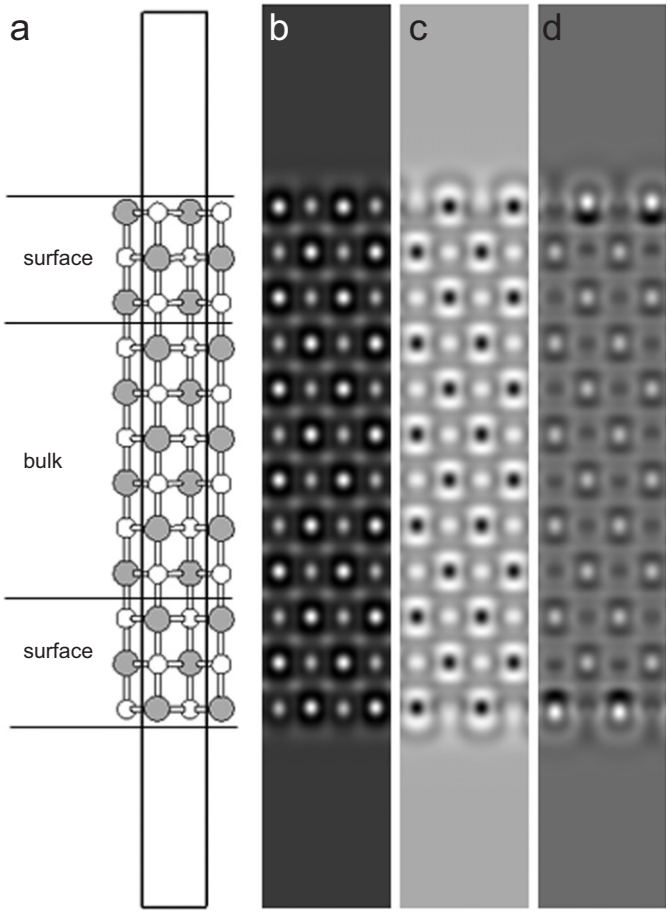

Fig. 2. The 13-layer structure of MgO (1 0 0) (a) and its image I(scf) (b), image I(scf-neu) (c), and image I(scf-ion), for an aberration corrected Jeol2200FS. The image ranges are 0.4693 to 2.8553 for (b), −0.1102 to 0.0547 for (c), and −0.0352 to 0.0483 for (d). The thickness is 10 unit cells thick (about 60 Å).

Table 1). For the MgO Rt3 structure, the contrast changes found were 10–60%; while values ranging from 5% to 20% for the MgO (1 0 0) structure were observed (with a singular exception at defocus −150 Å for the H9000 microscope). Note that the parameters for the ion scattering factors are fitted to bulk MgO. Since MgO Rt3 is a polar structure with a reconstructed surface, large deviations from bulk MgO are expected. In contrast, the MgO (1 0 0) structure exhibits no surface reconstruction, which suggests it more closely resembles the bulk MgO structure. It is also found that there are no apparent differences in contrast changes from bulk and surface layers (also in Supplementary Table 1).

3.2. Charge transfer relative to neutral atoms

Images simulated from F^{e}_{neu} and F^{e}_{scf} represent the neutral atoms model and our DFT model. As a result, the image difference map is a measure of the charge transfer with respect to the neutral atoms reference. The largest change is $Mg \xrightarrow{-2e} Mg^{2+}$ and $O \xrightarrow{+2e} O^{2-}$ since Mg and O are almost fully oxidized into Mg^{2+} and O^{2-} in bulk MgO. As shown in Fig. 1(a), the MgO Rt3 structure consists of alternating Mg and O layers. In the Mg layers, the Coulomb potential is increased after charge transfer; whereas it is decreased in the O layers. From our previous studies, the contrast in a difference image is known to be enhanced if the atoms are aligned in different columns, as is the case for the [1 1 0] orientation in both the MgO Rt3 and MgO (1 0 0) structure profile images.

The contrast due to charge transfer at the surface contributes about 10–30% of the overall contrast for the MgO Rt3 images and 5–30% for the MgO (1 0 0) images,

depending on the choice of imaging parameters (see Supplementary Table 2). Contrast variation of this order should be readily detectable experimentally. Additionally, the contrast in different regions of the slab was analyzed for both bulk and surface layers, and was shown to also contribute significant charge transfer contrast in the difference maps.

3.3. Charge transfer relative to ions

As mentioned, MgO is close to an ideal ionic compound, so neutral atoms are not particularly representative of the bulk structure factors. An alternative and more appropriate approach is to reference against ions, i.e. comparing images simulated from F^{e}_{scf} and F^{e}_{ion}, which should eliminate bulk effects and provide a more local representation of the charge defects at the surface. A typical difference image I(scf-ion) for MgO Rt3 is shown in Fig. 1(d). In the bulk layers, only a small contrast in the difference image I(scf-ion) is observable. The contrast in the surface layers is considerably larger owing to the presence of charge defects in the near-surface region. A bright spot is clearly discernable under the dangling Mg in the I(scf-ion) image, which corresponds to its complimentary dark spot in the I(scf-neu) image. Therefore the charge on Mg is between 0 and +2, consistent with our DFT results (+1.65). In the second layer, there are two flavors of oxygen: (1) where oxygen is under the dangling Mg, and (2) where oxygen is dangling at the surface. By comparing images, I(scf-ion) and I(scf-neu), with the model structure, we conclude that the holes are localized between the dangling Mg atoms and the O atoms beneath them. The dangling O in the second layer is not fully oxidized to O^{2-}, which is also in agreement with our DFT results (−1.52). From Fig. 1(d), we can also see that there is a bright contrast delocalized around the two dangling O atoms.

For comparison, the contrast values for different imaging parameters are tabulated for the charge defect-free structure, MgO (1 0 0) in Table 1. Since the MgO (1 0 0) surface is non-polar and has no charge defects in the surface layers, the contrast in the bulk and surface layers is almost the same (differences of 2–9%). This indicates that the effects due to redistribution of electrons in the absence of additional charge defects are quite small, and unlikely to be easily (if at all) experimentally observable. It is worth mentioning that the contrast in the bulk layers is much smaller than at the surface (cf. Table 1). This result can be attributed to the exchange-correlation potentials used in our calculations, which do not exactly replicate those used in the fitting of the ion parameters.

3.4. Imaging parameter

In the previous two sections, we have demonstrated that in principle it should be possible to observe charge transfer and charge defects at a planar boundary, a crystal surface. In this section, we will explore defocus and thickness effects on the image contrast in order to determine optimal imaging conditions.

A through-focal series of MgO Rt3 [1 1 0] images is shown in Figs. 3 and 4. The contrast percentages relative to

Table 1
The contrast ratios of σ(scf-ion)/σ(scf) with different defocus in bulk and surface layers

Defocus (Å)	MgO Rt3 surface profile image		MgO (1 0 0) surface profile image	
	Bulk	Surface	Bulk	Surface
Jeol 2200 microscope				
−160	6.2%, 0.2498	22%, 0.2922	2.5%, 0.4596	4.4%, 0.4305
−140	7.2%, 0.2201	21%, 0.2665	2.3%, 0.5045	4.2%, 0.4731
−120	8.3%, 0.1813	21%, 0.2314	2.2%, 0.5563	3.9%, 0.5137
−100	6.8%, 0.1972	18%, 0.2177	2.0%, 0.5849	3.6%, 0.5322
−80	4.6%, 0.2268	14%, 0.2118	2.0%, 0.5518	3.3%, 0.5005
−60	3.5%, 0.2024	12%, 0.1714	2.0%, 0.4604	3.0%, 0.4215
−40	3.4%, 0.1216	14%, 0.0960	1.9%, 0.3736	2.6%, 0.3532
−20	3.0%, 0.1000	12%, 0.0983	1.6%, 0.3761	2.3%, 0.3713
0	2.9%, 0.1728	9.5%, 0.1744	1.5%, 0.4412	2.4%, 0.4401
H9000 UHV microscope				
−1200	43%, 0.1031	33%, 0.1419	1.1%, 0.0415	3.4%, 0.4305
−1050	36%, 0.0963	34%, 0.1304	4.3%, 0.0424	4.8%, 0.4731
−900	20%, 0.0877	35%, 0.1504	1.7%, 0.0444	5.1%, 0.5137
−750	9.4%, 0.1203	32%, 0.2044	3.0%, 0.0451	4.6%, 0.5322
−600	19%, 0.0348	33%, 0.2376	4.6%, 0.0420	8.2%, 0.5005
−450	9.8%, 0.1152	27%, 0.2681	2.5%, 0.0351	6.0%, 0.4215
−300	13%, 0.0370	21%, 0.1906	1.5%, 0.0276	5.0%, 0.3532
−150	14%, 0.0938	17%, 0.0917	8.4%, 0.0242	7.3%, 0.3713
0	16%, 0.0727	24%, 0.1249	2.3%, 0.0268	7.2%, 0.4401

The thickness is about 52 Å for MgO Rt3 surface and about 60 Å for MgO (1 0 0) surface.

ions and neutral atoms are also tabulated in the Table 1 and Supplementary Table 2. It is clear that relative to the neutral atoms, the bulk layers contribute significantly more contrast in aberration-corrected HREM images. Although a conventional H9000 microscope cannot quite achieve atomic resolution along this direction, it is rather more sensitive to the effects at the surface. This is to be expected since there is more contrast transfer at small scattering angles. The surface sensitivity is shown in the Supplementary Table 2, where the bulk layers contribute much less contrast than do surface layers in the H9000 HREM images. However, the contrast from bulk layers is consistently much less than that from surface layers (containing charge defects) in both the Jeol 2200 and H9000 images.

Throughout this work the defocus has been shown to have a significant effect on image contrast. Since the optimum Scherzer defocus is only about -35 Å for Jeol 2200 under the C_c-limited condition [23] and -430 Å for the H9000, we used a broader defocus window for H9000. The resulting contrast ratios σ(scf-neu)/σ(scf) and σ(scf-ion)/σ(scf) are therefore larger in the simulated H9000 images. The general trend is that a larger defocus leads to improved contrast ratios for Jeol 2200 images; while such a trend is not obvious in simulated H9000 images. As the defocus becomes too large, the images often become difficult to interpret directly although part of this will be delocalization effects with the relatively small slabs that were used for both the DFT and multislice/image simulation. We find that a defocus of -120 Å for the Jeol 2200 and a defocus of -900 Å for the H9000 give a reasonable compromise between contrast ratio and image quality. (Of course, the ''optimum'' defocus will depend upon the spacings in the samples so these numbers should not be overinterpreted.)

In typical HREM experiments, a thinner specimen is usually far better for analysis than a thicker one. However, for studies of this nature, if the specimen is too thin it might be difficult to observe charge transfer and charge defects.

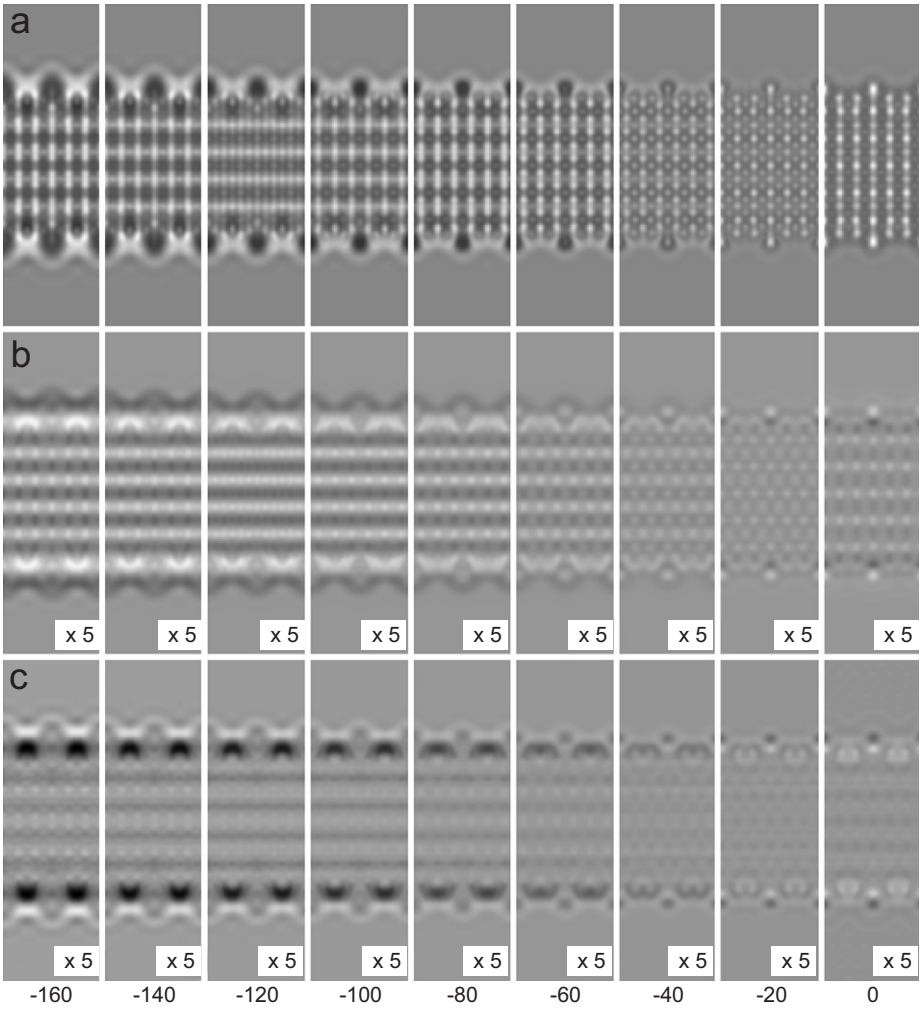

Fig. 3. Simulated through-focal series of difference images for MgO Rt3 [1 1 0] using a Jeol2200FS-aberration corrected microscope. The images I(scf) (a), I(scf-neu) (b), and I(scf-ion) (c) are all for a thickness of 10 unit cells (about 52 Å) from a defocus of -160 to 0 Å with a step size of 20 Å. The image contrast for I(scf-neu) and I(scf-ion) images is enhanced by a scaling factor of 5. The overall contrast range is -0.81543 to 0.92189.

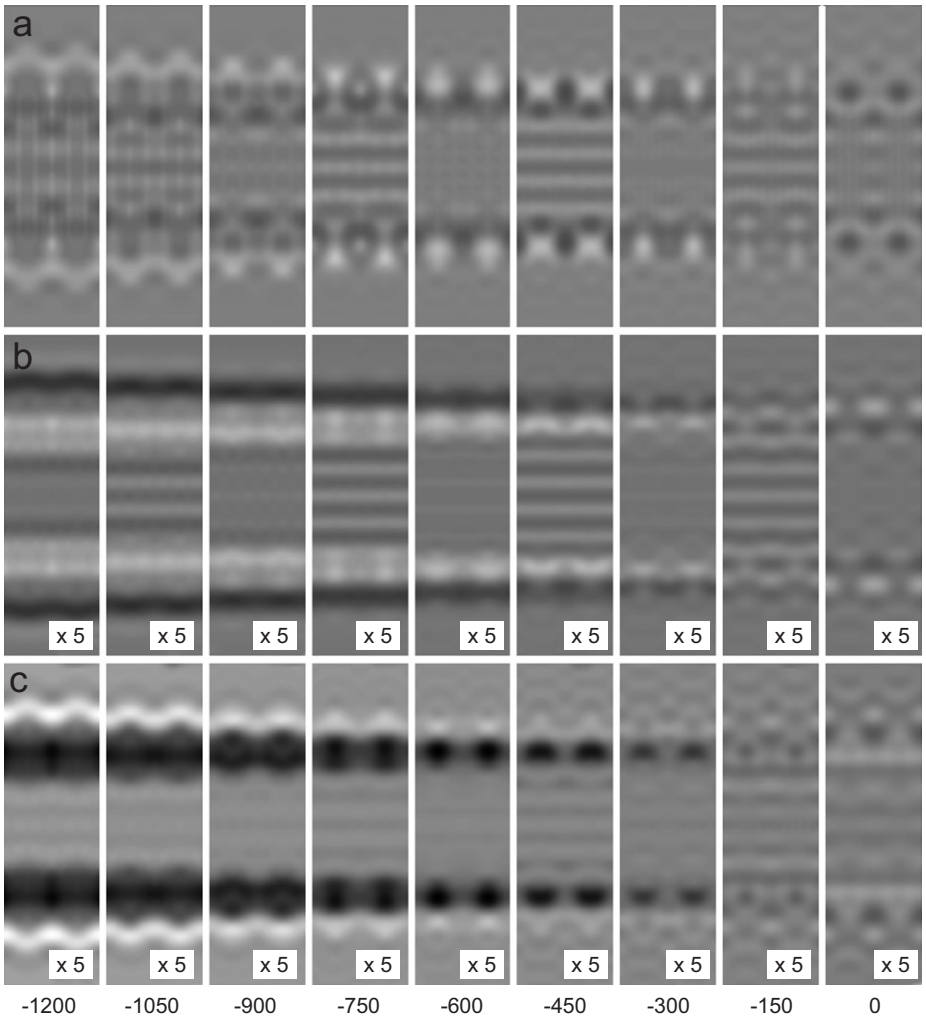

Fig. 4. Simulated through-focal series for MgO Rt3 [1 1 0] for an H9000 microscope. The images I(scf) (a), I(scf-neu) (b), and I(scf-ion) (c) are all for a thickness of 10 unit cells (about 60 Å) from a defocus of −1200 to 0 Å with a step size of 150 Å. The image contrast of I(scf-neu) and I(scf-ion) images is enhanced by a scaling factor of 5. The overall contrast range is −1.03971 to 1.48935.

Table 2 and the supplementary tables list contrast percentages for charge transfer and charge defects with thicknesses ranging from 1 to 60 unit cells for the MgO Rt3 structure and 1–80 unit cells for the MgO (1 0 0) structure. While the effect of thickness is small compared with the effect of defocus, thicker specimens do increase contrast ratios as expected. When the sample thickness increases from 1 unit cell to 60 unit cells in the simulated Jeol 2200 images, the surface contrast ratios increase from 18% to 25% for σ(scf-neu)/σ(scf) and from 19% to 51% for σ(scf-ion)/σ(scf). As a general rule, dynamic scattering is increased for thicker samples, and again a competition between optimal contrast and straightforward image interpretation arises. The tradeoff between image interpretation at large crystal thicknesses and contrast is apparent in Fig. 5. In this case, we conclude that the optimum thickness is about 20 unit cells ($\approx$103 Å) for the MgO Rt3 structure and about 40 unit cell ($\approx$120 Å) for the MgO (1 0 0) structure.

4. Discussion

The results that we have obtained strongly suggest that imaging local charge defects should be very possible using HREM. For the MgO Rt3 example, the contrast due to charge transfer and charge defects was at least 20% of the overall contrast under optimized imaging conditions, which is much larger than the contrast (about 10%) due to charge transfer in our previous studies on bulk oxides [16]. Contrast of this magnitude should definitely be detectable experimentally, although we acknowledge that this will be different for different material systems. For instance, the MgO (1 0 0) structure would not appear to be a good candidate structure for experimental analysis. Table 3 shows the calculated charges for the two model structures via Bader's "atom in molecule" (AIM) analysis [24], which is based on the topology of charge density. (Note that there is no good way to partition to different atoms electron density numbers from a density-functional based such as

Table 2
The contrast ratios of σ(scf-ion)/σ(scf) and the contrast σ(scf) with different thickness in bulk and surface layers

Thickness (Unit cell)	Jeol 2200 microscope		H9000 UHV microscope	
	Bulk	Surface	Bulk	Surface
MgO Rt3 surface profile image				
1	7.0%, 0.0212	19%, 0.0261	33%, 0.0095	34%, 0.0149
5	7.5%, 0.0973	19%, 0.1266	28%, 0.0460	33%, 0.0761
10	8.3%, 0.1813	21%, 0.2314	20%, 0.0876	35%, 0.1504
15	8.2%, 0.2890	23%, 0.3169	13%, 0.1262	41%, 0.2164
20	8.4%, 0.3918	26%, 0.3782	10%, 0.1644	50%, 0.2738
40	22%, 0.3133	46%, 0.3623	31%, 0.3286	91%, 0.4587
60	60%, 0.2672	51%, 0.4653	35%, 0.3913	120%, 0.5116
MgO (1 0 0) surface profile image				
1	2.7%, 0.0336	4.6%, 0.0323	1.0%, 0.0133	7.0%, 0.0128
5	2.6%, 0.1659	4.5%, 0.1584	0.98%, 0.0693	6.6%, 0.0659
10	2.4%, 0.3213	4.2%, 0.3032	1.1%, 0.1404	6.0%, 0.1330
20	2.2%, 0.5563	3.9%, 0.5137	1.6%, 0.2579	5.0%, 0.2477
40	5.5%, 0.5590	8.0%, 0.5143	3.9%, 0.4103	4.9%, 0.4131
60	6.5%, 0.6633	8.8%, 0.6764	4.1%, 0.5876	7.2%, 0.5785
80	4.8%, 1.0305	8.2%, 0.9715	5.3%, 0.5509	12%, 0.5501

The defocus is −120 Å for Jeol 2200 microscope and −900 Å for H9000 microscope.

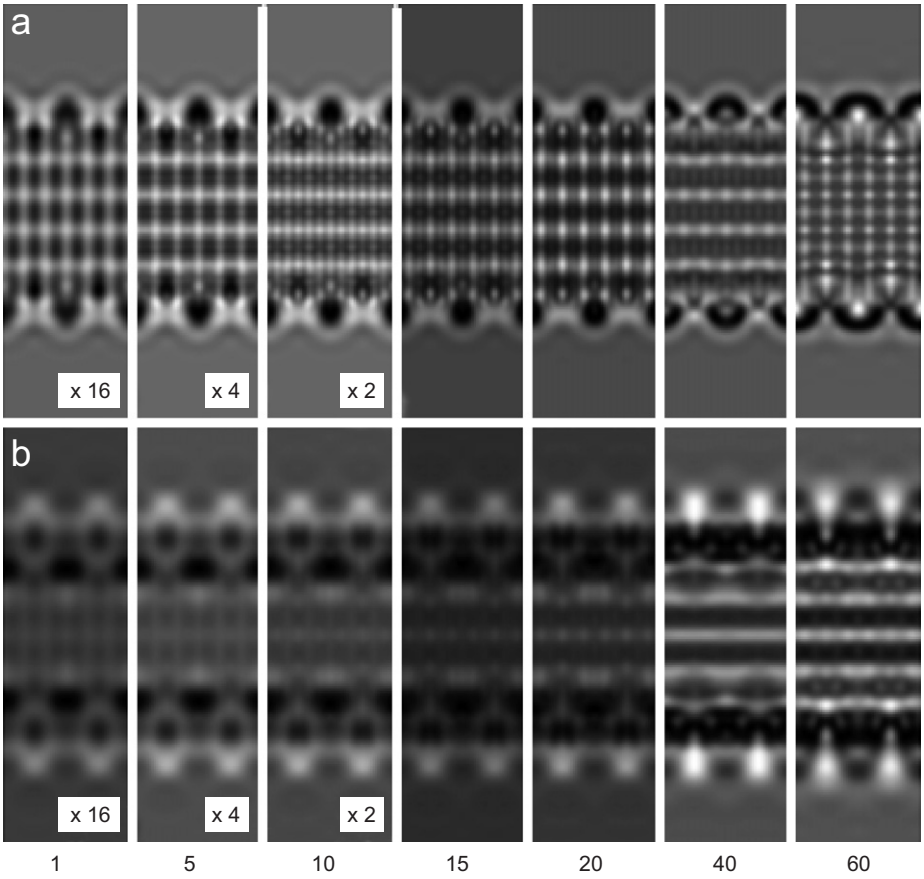

Fig. 5. Images *I*(scf) for MgO Rt3 [1 1 0] simulated with a defocus of −120 Å for a Jeol2200FS microscope (a) and with a defocus of −900 Å for a H9000 microscope (b) with different thickness from 1 to 60 unit cells (about 5.2–312 Å). The scaling factor for the image contrast is indicated at bottom right. The overall contrast range is 0.000–2.28085.

Table 3
Charges calculated by Bader's "atom in molecule" (AIM) analysis[a]

Layer	MgO Rt3 structure	MgO (1 0 0) structure
1	Mg: 1.649(8)	Mg: 1.714(8); O: −1.709(6)
2	O: −1.482(6)	Mg: 1.713(7); O: −1.717(8)
3	Mg: 1.695(9)	Mg: 1.716(7); O: −1.714(8)
4	O: −1.617(5); O: −1.659(5)	Mg: 1.716(8); O: −1.715(8)
5	Mg: 1.690(5)	Mg: 1.716(7); O: −1.715(8)
6	O: −1.673(4)	Mg: 1.716(7); O: −1.715(8)
7	Mg: 1.687(5)	

[a]In bulk MgO, the calculated AIM charges for Mg and O are 1.710(3) and −1.710(3).

we have used here, the AIM method is one convention which can be used to compare different atoms—it should not be interpreted as an absolute measure of the ionicity.) The charges on Mg and O in the MgO (1 0 0) structure are close to those in the bulk MgO material (about ± 1.71). In the MgO Rt3 structure, the charge on the outermost Mg is less than in the bulk (1.65), the oxygen in the second layer substantially reduced (−1.45). The charge defects in the surface layers also have effects in deeper layers, as we can see that the charges on Mg and O below are only about ± 1.69 with in general an exponential decay towards the bulk value with distance from the surface. This explains why σ(scf-ion)/σ(scf) for the bulk layers in the MgO Rt3 structure is much larger than that in the MgO (1 0 0) structure.

One experimental caveat may be the so-called Stobbs factor [25,26], but this appears to only be a discrepancy in the absolute contrast of some experimental versus calculated images. For a local charge defect one automatically has an experimental reference, the bulk material. If one calculates the difference in the image contrast at a defect (interface or surface) and that in the bulk, to a large extent the Stobbs factor should cancel out. The key experimental issue will be obtaining good enough samples without wildly varying thicknesses and/or high concentrations of other defects such as those due to ion-beam thinning; this will not be a trivial task. While we could speculate more, probably at this stage experimental tests are more important.

Acknowledgments

This work was supported by the DOE on Grant No. DE-FG02-01ER45945/A006.

Appendix A. Supplementary Materials

Supplementary data associated with this article can be found in the online version at doi:10.1016/j.ultramic.2006.10.001.

References

[1] J.M. Zuo, J.C.H. Spence, M. O'Keeffe, Phys. Rev. Lett. 61 (1988) 353.
[2] J.M. Zuo, J.C.H. Spence, Ultramicroscopy 35 (1991) 185.
[3] K. Gjonnes, N. Boe, Micron 25 (1994) 29.
[4] M. Saunders, P.A. Midgley, R. Vincent, Inst. Phys. Conf. Ser. 147 (1995) 125.
[5] M. Saunders, P. Midgley, R. Vincent, J. Steeds, J. Electron Microsc. 45 (1996) 11.
[6] R. Holmestad, C.R. Birkeland, Philos. Mag. A: Phys. Condens Matter: Struct. Defects Mech. Properties 77 (1998) 1231.
[7] W. Nuechter, A.L. Weickenmeier, J. Mayer, Phys. Stat. Sol. A: Appl. Res. 166 (1998) 367.
[8] R. Holmestad, C.R. Birkeland, K. Marthinsen, R. Hoier, J.M. Zuo, Microsc. Res. Tech. 46 (1999) 130.
[9] M. Saunders, G. Fox, P.A. Midgley, Acta Crystallogr. Section A: Found. Crystallogr. A 55 (1999) 471.
[10] J.M. Zuo, M. Kim, M. O'Keeffe, J.C.H. Spence, Nature (London) 401 (1999) 49.
[11] B. Jiang, J.M. Zuo, Q. Chen, J.C.H. Spence, Acta Crystallogr. Section A: Found. Crystallogr. A 58 (2002) 4.
[12] B. Jiang, J.M. Zuo, N. Jiang, M. O'Keeffe, J.C.H. Spence, Acta Crystallogr. Section A: Found. Crystallogr. A 59 (2003) 341.
[13] J.M. Zuo, Rep. Prog. Phys. 67 (2004) 2053.
[14] A. Subramanian, L.D. Marks, O. Warschkow, D.E. Ellis, Phys. Rev. Lett. 92 (2004) 026101/1.
[15] A. Subramanian, L.D. Marks, P. Blaha, O. Warschkow, D.E. Ellis, in preparation, 2006.
[16] B. Deng, L.D. Marks, Acta Crystallogr. Section A 62 (2006) 208.
[17] D. Waasmaier, A. Kirfel, Acta Crystallogr. Section A: Found. Crystallogr. A 51 (1995) 416.
[18] J.-M. Gillet, P. Cortona, Phys. Rev. B: Condens. Matter Mater. Phys. 60 (1999) 8569.
[19] P. Blaha, K. Schwarz, P. Sorantin, S.B. Trickey, Comput. Phys. Commun. 59 (1990) 399.
[20] P. Blaha, K. Schwarz, G.K.H. Madsen, D. Kvasnicka, J. Luitz, WIEN2k, An Augmented Plane Wave + Local Orbitals Program for Calculating Crystal Properties, Vienna University of Technology, Vienna, 2001.
[21] J.P. Perdew, K. Burke, Y. Wang, Phys. Rev. B: Condens. Matter 54 (1996) 16533.
[22] L.D. Marks, Ultramicroscopy 38 (1991) 325.
[23] L.Y. Chang, F.R. Chen, A. Kirkland, I.K.J. Jung, J. Electron Microsc. 52 (2003) 359.
[24] R.F.W. Bader, Atoms in Molecules: A Quantum Theory, Clarendon Press, Oxford, 1990.
[25] M.J. Hytch, W.M. Stobbs, Microsc. Microanal. Microstruct. 5 (1994) 133.
[26] C.B. Boothroyd, J. Microsc.—Oxford 190 (1998) 99.